*JOURNAL OF PHYSICAL CHEMISTRY, 2025, Vol. 99, No. 1, c. 112–124*

## CHEMOINFORMATICS AND COMPUTER MODELING

# ON APPLICABILITY OF EMBEDDED ATOM MODEL (EAM) POTENTIALS TO LIQUID SILICON AND GERMANIUM

**D. K. Belashchenko**

*National University of Science and Technology (MISiS), Moscow, Russia*

*e-mail: dkbel75@gmail.com*

Received March 13, 2024
Revised March 13, 2024
Accepted April 02, 2024

**Abstract.** Potentials of the embedded atom model (EAM) for liquid silicon and germanium are proposed. The potentials are calculated from diffraction data using the Schommers algorithm and presented in the form of tables and piecewise continuous polynomials. Each pairwise contribution to the potential has a form close to a hard-sphere one with a step down. The properties of liquid Si and Ge at temperatures up to 2000 K are calculated, viz. the density, energy, bulk modulus, and self-diffusion coefficients. The agreement with the experiment is noted to be good. The bond direction is found to almost completely disappear after melting for ordinary densities of liquid Si and Ge. The bond direction is assumed to be able to appear at heating and when the density of melts is decreased by 2–3 times.

**Keywords**: *liquid silicon, germanium, bond direction, density, energy, compressibility, self-diffusion*

**DOI: 10.31857/S00444537250112e5**

## INTRODUCTION

Below, we consider the problem of computer simulation of liquids resulted from melting and partial metallization of substances with the covalent bond. Such simple substances are located in the band of the Periodic System including silicon and germanium (Group 4), antimony (Group 5), and tellurium (Group 6). Most of these substances, including silicon and germanium, are semiconductors in the solid state and exhibit metallic properties in the liquid state. In the case of antimony, the contribution of the covalent bond in the crystal is small while in tellurium the covalency is quite significant. To simulate crystalline covalent substances, one usually apply potentials that boost orientation (presence of valence angles). However, in the liquid state, signs of orientational interaction are not always observed. Therefore, the question arises whether one and the same interparticle potential can be applied when simulating such a system in both crystalline and liquid states. If the bond types in the crystal and in the liquid are really different, the interparticle interaction potentials should be different. This is indicated, in particular, by *ab initio* calculations, which show dramatic differences in the structure of the crystal and liquid.

Although there have been quite frequent attempts to apply unified potentials for crystal and liquid in the case of silicon and germanium, good results have not been achieved. Below, we consider ways to simulate these substances in the liquid state with the usual spherically symmetric potentials used for metals.

## EAM INTERPARTICLE POTENTIALS FOR SILICON AND GERMANIUM

**Simulating silicon.** Solid silicon is a semiconductor. The crystalline lattice of silicon is cubic with a coordination number CN = 4. Each atom is located at the center of the tetrahedron and connected to its neighboring atoms by covalent bonds of the $sp^3$ type. The length of this bond is 2.352 Å. Diffraction data on the structure of liquid silicon are given in the book by Y. Waseda [1], and for pressures of 4–23 GPa they are given in [2, 3]. The pair correlation function (PCF) of silicon for the temperature 1733 K is shown in Fig. 1. The first peak is quite high and narrow, so that the first coordination sphere is well defined; its radius is 3.05 Å. The average coordination number CN = 6.24 ± 1.45. There are data on the density of solid and liquid silicon up to 2000 K [4, 5], silicon energy up to 3600 K [6, 7], compressibility [8, 9], self-diffusion coefficients [3, 10], behavior at high pressures [3, 11, 12], etc.

To simulate substances with the diamond lattice — carbon, silicon, germanium — by the molecular dynamics (MD) method, a number of interparticle potentials have been proposed that realize the directionality of bonding, viz. Stillinger-Weber (SW) [13–15], Tersoff (Ter) [16–18] and others that depend on the local

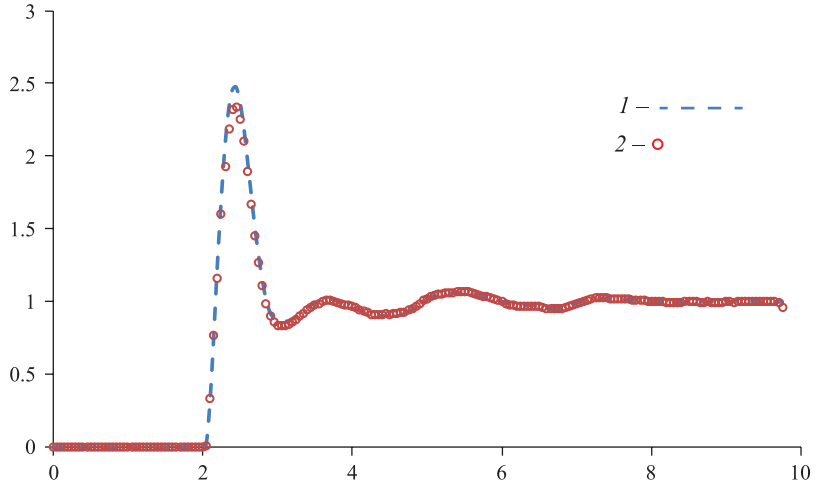


**Fig. 1.** Pair correlation function of Si at 1773 K — (1) diffraction data [1], and (2) EAM potential model.

structure, such as environment dependent interatomic potential (EDIP) [12, 19, 20]. Such potentials include valence angles between the nearest four neighbors of the central atom, which allows implementing the tetrahedral configuration. A significant number of potentials are reported in [21] and given in the NIST repository [22]. Potentials that take valence angles into account are usually used to calculate the structure, diffusion coefficients, and melting points rather than energy characteristics. M. Baskes et al. [23, 24] applied the modified embedded atom model (MEAM) potential for non-isotropic substances. The *ab initio* method is quite widely used [17, 21]. Data obtained by this method were used to calculate potentials by a Potfit-type program [25, 26]. The mentioned works mainly deal with the models of crystalline silicon and its alloys.

The transition to analyzing liquid silicon causes difficulties due to a significant change in the bond type. In the case of SW and Ter potentials, the maximum number of atoms of the model has CN = 6 (44% of atoms for SW and 33% for Ter), and the number of atoms with CN = 4 is small, viz. 7% in SW and 8% in Ter, see Fig. 3 in [17]). The calculated melting points of silicon with these potentials are 1400 and 2750 K (the actual value is 1687 K), respectively. Under these conditions, using the SW and Ter potentials is questionable. As for the MEAM potential, it was not used for liquid silicon in [23, 24].

In this connection, in this work, we propose the potential of the embedded atom model (EAM [27]) for liquid silicon using diffraction data. The potential energy of the metal is written as

$$U = \sum_i \Phi(\rho_i) + \sum_{i<j} \phi(r_{ij}). \qquad (1)$$

Here, $\Phi(\rho_i)$ is the imbedding potential of the $i$th atom, which depends on the "effective electron density" $\rho$ at the location of the atom center, and the second sum over pairs of atoms contains the usual pair potential. The effective electron density at the location of the atom is created by the surrounding atoms and determined by the formula

$$\rho_i = \sum_j \psi(r_{ij}) \qquad (2)$$

where $\psi(r_{ij})$ is the contribution to the electron density of the atom $i$ by neighbor number $j$. Three fitting functions $\Phi(\rho)$, $\varphi(r)$, and $\psi(r)$ are used in the calculations, so that the possibilities of matching the calculated properties with experimental values are very broad.

To find the pair contribution $\varphi(r)$, we apply the Schommers algorithm [28, 29], in which the correction to the current version of the pair contribution to the potential is determined by the difference between the diffraction and PCF models. Below, we define the distance between the two plots — the PCF histograms $g_0(r_i)$ and $g(r_i)$ — through the residual $R_g$

$$R_g = \left\{ \frac{1}{n_2 - n_1 + 1} \sum_{n_1}^{n_2} \left[ g_0(r_j) - g(r_j)^2 \right] \right\}^{1/2}, \qquad (3)$$

where $g_0(r_j)$ is the histogram of the objective PCF, $g(r)$ is the histogram of the PCF model, $n_1$ and $n_2$ are the summation boundaries of the tabular data, and $j$ is the element number of the PCF histogram. At first, we used Y. Waseda's PCF [1] to construct, using the Schommers algorithm, a model of liquid silicon at 1733 K with a pair potential and a very small residual $R_g = 0.023$ (see Fig. 1). The resulting pair contribution to the EAM potential is given in Table 1 and Fig. 2

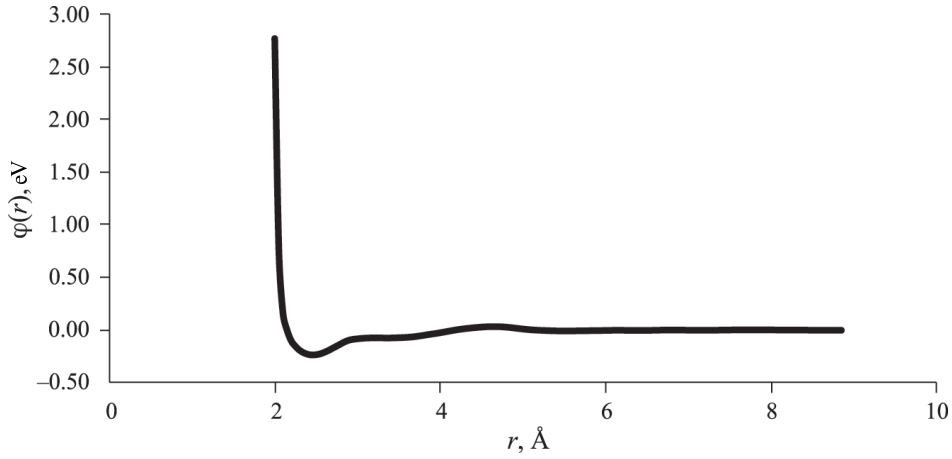


**Fig. 2.** Pair contribution to the EAM potential of liquid silicon. Schommers algorithm.

with the step $dr = 0.05$ Å. It resembles a hard-sphere one with a step downward. The radius of the cut-off is $r_c = 8.855$ Å.

The embedded potential is of the form

$$\psi(r) = p_1 \exp(-p_2 r), \quad \rho_0 = 1,$$
$$\Phi(\rho) = a_1 + c_1(\rho - \rho_0)^2 \quad \text{for} \quad \rho_1 \le \rho \le \rho_2, \quad (4)$$
$$\Phi(\rho) = a_2 + b_2(\rho - \rho_1) + c_2(\rho - \rho_1)^2.$$

The coefficients $a_2$ and $b_2$ are related to $a_1$ and $c_1$ by the condition of continuity of the function $\Phi(\rho)$ and its derivative: $a_2 = a_1 + c_1(\rho_1-\rho_0)^2$ and $b_2 = 2c_1(\rho_1-\rho_0)$. The values $a_1$, $c_1$, $c_2$, $\rho_{11}$ must be given. The parameters of the EAM embedded potential $\Phi(\rho)$ are given in Table 2. The values $\rho > \rho_2$ can be obtained only in highly compressed states.

Using the EAM potential, we constructed a series of models of liquid silicon consisting of 2048 atoms in a basic cube with periodic boundary conditions, at temperatures of 1690–2000 K, in *NVT* and *NpT* modes. The pair correlation function $g(r)$ at 1733 K is shown in Fig. 1 in excellent agreement with diffraction data [1].

The CN distribution of the silicon model shown in Fig. 3 has the form characteristic of dense packings, and CN = 4 is not prominent in any way. This distribution is close to the one obtained by the *ab initio* method at 1800 K [21]. Chain or tetrahedral packing is not visible in liquid silicon. Melting destroys the network structure.

The distribution of azimuthal angles (Fig. 4) is also not similar to the case of the Ter potential [17, 30], where one can see an acute maximum at angles of ~60°. *Ab initio* calculations [21] lead to a curve with two maximums for the angles 60° and 90°, as in the case of EAM (Fig. 4); however, the right maximum at 90° in [21] is slightly higher than the left peak. The SW and Ter potentials lead to angular distributions that differ greatly in shape from the curve in Fig. 4.

The results of calculations of liquid silicon properties at temperatures up to 2000 K are given in Table 3. As we can see from the table, the EAM potential allows obtaining the correct dependence of the liquid silicon density on temperature up to 2000 K, good agreement of the PCF with the experiment at 1733 K (Fig. 1), and good agreement of the modulus of compression with the experiment. At 1733 K, the heat capacities $C_v$ and $C_p$ of the silicon model were 16.9 and 21.4 J/(mol K). The adiabatic modulus $K_s = 35.7$ GPa [8, 9] was recalculated to the isothermal one $K_T$ given the ratio of heat capacities $C_p/C_v = 1.266$; as a result, $K_T = 28.2$ GPa. For the value $c_1 = 2.05$ eV, the modulus value found from the pressure-volume relationship is $K_T = 30.6$ GPa. Upon heating from 1690 to 2000 K, the modulus $K_T$ decreases rather slowly, by only 10%. Good agreement with the experiment [7] is obtained for the energy of liquid silicon. With the temperature increasing, a slight reduction in the energy of the models is observed due to the failure to take into account the electronic heat capacity of the silicon models. The electronic heat is ~2 J/(mol K) capacity for 1600–2000 K.

The self-diffusion coefficient $D$ was found from the time dependence of the mean square of the particle displacement. The EAM potential yields high values of the coefficient $D \sim 2 \times 10^{-4}$ cm$^2$/s (Table 3). The *ab initio* method yields the value $D = 2.26 \times 10^{-4}$ of the same order [21, 32]. However, the SW and Ter potentials result in self-diffusion coefficients of liquid silicon of the order of $10^{-5}$ cm$^2$/s [30, 33]. The effect of increased self-diffusion coefficient (up to ~$10^{-4}$ cm$^2$/s) was observed earlier for liquid antimony models for $T > 1000$ K [34], but it gradually disappears upon heating.

**Table 1.** Pair contributions to the liquid silicon potential. Schommers algorithm at 1733 K. Pair correlation function [1], residual $R_g = 0.023$

| $r$, Å | φ($r$), eV | $r$, Å | φ($r$), eV | $r$, Å | φ($r$), eV | $r$, Å | φ($r$), eV |
|---|---|---|---|---|---|---|---|
| 1.5 | 122.291000 | 3.35 | −0.073576 | 5.2 | −0.000563 | 7.05 | −0.000178 |
| 1.55 | 101.294000 | 3.4 | −0.073472 | 5.25 | −0.002079 | 7.1 | −0.000617 |
| 1.6 | 82.287700 | 3.45 | −0.072458 | 5.3 | −0.003564 | 7.15 | −0.000834 |
| 1.65 | 65.261100 | 3.5 | −0.071103 | 5.35 | −0.005022 | 7.2 | −0.000750 |
| 1.7 | 50.214400 | 3.55 | −0.069557 | 5.4 | −0.006002 | 7.25 | −0.000432 |
| 1.75 | 37.180300 | 3.6 | −0.067373 | 5.45 | −0.006646 | 7.3 | 0.000022 |
| 1.8 | 26.239600 | 3.65 | −0.064463 | 5.5 | −0.007191 | 7.35 | 0.000467 |
| 1.85 | 17.473600 | 3.7 | −0.060170 | 5.55 | −0.007183 | 7.4 | 0.001153 |
| 1.9 | 10.839500 | 3.75 | −0.054712 | 5.6 | −0.006751 | 7.45 | 0.001830 |
| 1.95 | 6.067210 | 3.8 | −0.048719 | 5.65 | −0.005952 | 7.5 | 0.002192 |
| 2.00 | 2.767880 | 3.85 | −0.042092 | 5.7 | −0.005362 | 7.55 | 0.002491 |
| 2.05 | 0.755346 | 3.9 | −0.036168 | 5.75 | −0.005026 | 7.6 | 0.002586 |
| 2.1 | 0.159373 | 3.95 | −0.030396 | 5.8 | −0.004385 | 7.65 | 0.002628 |
| 2.15 | −0.001554 | 4.00 | −0.023942 | 5.85 | −0.003832 | 7.7 | 0.002827 |
| 2.2 | −0.101008 | 4.05 | −0.016892 | 5.9 | −0.003009 | 7.75 | 0.002638 |
| 2.25 | −0.152195 | 4.1 | −0.009745 | 5.95 | −0.002833 | 7.8 | 0.002702 |
| 2.3 | −0.189574 | 4.15 | −0.002723 | 6 | −0.002206 | 7.85 | 0.002747 |
| 2.35 | −0.213938 | 4.2 | 0.003849 | 6.05 | −0.001500 | 7.9 | 0.002539 |
| 2.4 | −0.228382 | 4.25 | 0.009620 | 6.1 | −0.000687 | 7.95 | 0.002463 |
| 2.45 | −0.234435 | 4.3 | 0.014813 | 6.15 | −0.000636 | 8 | 0.002386 |
| 2.5 | −0.232160 | 4.35 | 0.019150 | 6.2 | −0.000856 | 8.05 | 0.002338 |
| 2.55 | −0.224053 | 4.4 | 0.023231 | 6.25 | −0.001311 | 8.1 | 0.002013 |
| 2.6 | −0.209804 | 4.45 | 0.026716 | 6.3 | −0.001707 | 8.15 | 0.001976 |
| 2.65 | −0.191907 | 4.5 | 0.029711 | 6.35 | −0.002199 | 8.2 | 0.001765 |
| 2.7 | −0.171074 | 4.55 | 0.032243 | 6.4 | −0.002325 | 8.25 | 0.001668 |
| 2.75 | −0.150465 | 4.6 | 0.033630 | 6.45 | −0.002367 | 8.3 | 0.001353 |
| 2.8 | −0.129192 | 4.65 | 0.034171 | 6.5 | −0.001990 | 8.35 | 0.001162 |
| 2.85 | −0.108827 | 4.7 | 0.033699 | 6.55 | −0.001173 | 8.4 | 0.000972 |
| 2.9 | −0.094394 | 4.75 | 0.032001 | 6.6 | −0.000397 | 8.45 | 0.000613 |
| 2.95 | −0.086053 | 4.8 | 0.028947 | 6.65 | 0.000469 | 8.5 | 0.000282 |
| 3 | −0.081530 | 4.85 | 0.025344 | 6.7 | 0.001206 | 8.55 | 0.000034 |
| 3.05 | −0.077580 | 4.9 | 0.020481 | 6.75 | 0.001713 | 8.6 | −0.000053 |
| 3.1 | −0.074926 | 4.95 | 0.015896 | 6.8 | 0.002049 | 8.65 | −0.000177 |
| 3.15 | −0.073313 | 5 | 0.011360 | 6.85 | 0.001965 | 8.7 | −0.000182 |
| 3.2 | −0.073026 | 5.05 | 0.007204 | 6.9 | 0.001731 | 8.75 | −0.000497 |
| 3.25 | −0.072734 | 5.1 | 0.003855 | 6.95 | 0.000888 | 8.8 | −0.000248 |
| 3.3 | −0.073358 | 5.15 | 0.001455 | 7 | 0.000334 | 8.85 | 0.000000 |

**Table 2.** Liquid silicon. Parameters of the embedded potential Φ(ρ)

| | | | |
|---|---|---|---|
| $p_1$ | 0.46785 | $n$ | 2048 |
| $p_2$ | 0.80 | $dr$, Å | 0.05 |
| $r_1$ | 0.875 | $r_0$, Å | 9.86 |
| $r_2$ | 1.125 | $r_c$, Å | 8.855 |
| $a_1$, eV | −3.2823 | $c_1$, Å | 2.05 |

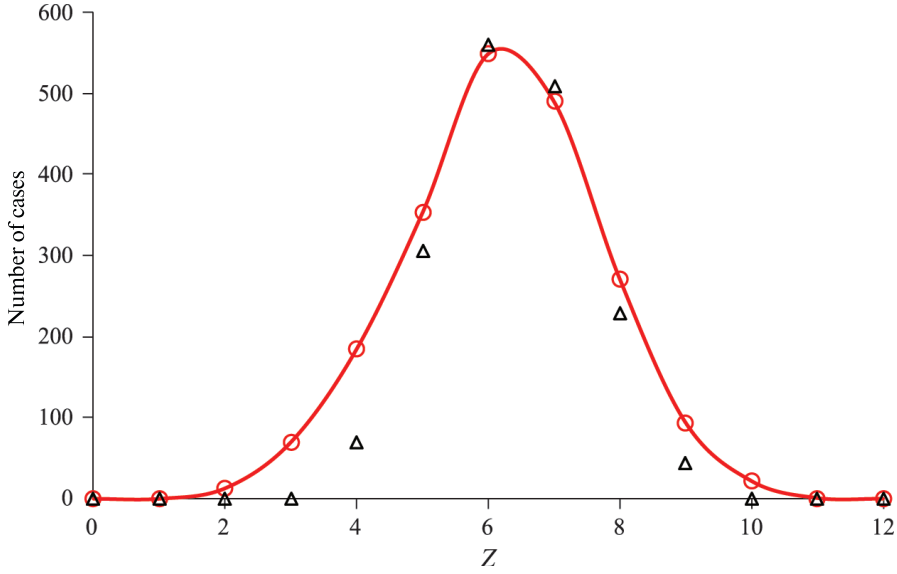


**Fig. 3.** The frequency of occurrence of the CN Z in the liquid silicon model at 1690 K. The radius of the coordination sphere is 3.05 Å — (*1*) EAM potential, and (*2*) 1800 K, *ab initio* method [21].

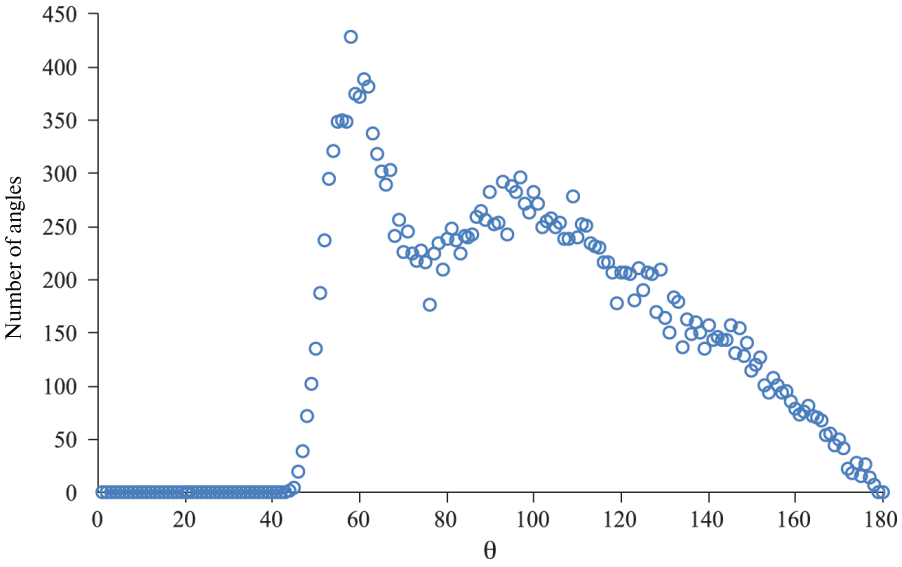


**Fig. 4.** Azimuth angles θ in the Si model at 1733 K.

The proximity of the silicon potential to the hard-sphere potential with a step down (Fig. 2) allows us to verify the formula for the self-diffusion coefficient of the hard-sphere model [35]

$$D_{\mathrm{HS}} = \left(D_0/n\right)\left(1 - n/1.09\right)\left(1 + n^2\left(0.4 - 0.83n^2\right)\right), \quad (5)$$

where $n = (N/V)\,\sigma^3$, $N$ is the number of particles in the volume $V$, σ is the sphere diameter, $m$ is its mass, $D_0 = (3/8)\sigma(k_{\mathrm{B}}T/\pi m)^{1/2}$. Multiplying the numerator and denominator of the fraction in the parentheses by Avogadro's number, we obtain, for $T$ = 1733 K, σ = 2.20 Å, $N/V$ = 0.053932 at/Å$^3$, $n$ = 0.5743, $D_0 = (3/8)\,2.2 \times 10^{-8} \times (8.31 \times 10^7 \times 1733/\pi/28.085)^{1/2} = 3.33 \times 10^{-4}$ cm$^2$/s, and finally $D_{\mathrm{HS}} = 2.86 \times 10^{-4}$ cm$^2$/s. This value agrees well with $2.65 \times 10^{-4}$ obtained by the MD method and with the value $D$ found by the *ab initio* method ($2.02 \cdot 10^{-4}$ cm$^2$/s for 1800°C [21]).

The self-diffusion mechanism can be refined by checking whether the Stokes-Einstein equation relating self-diffusion to viscosity holds for liquid silicon

$$D = \frac{kT}{6\pi\eta r_a}, \quad (6)$$

**Table 3.** Properties of Si models obtained by the MD method at $p$ ~0.001 GPa, $p_1$= 0.46785, $p_2$ = 0.800, $c_1$= 2.0500

| $T$, K | $d$, g/cm$^3$ | | | <ρ>[b] | $R_g$ | $-E$, kJ/mol | | $K_T$, GPa | | $D \times 10^5$, cm$^2$/s | |
|---|---|---|---|---|---|---|---|---|---|---|---|
| | MD | Exp. [4] | Exp. [5] | | | $-E_{MD}$ | $-E_{exp}$ [7] | MD | Exp. [9, 31] | MD | *Ab initio* [21, 32] |
| 1 | 2 | 3 | 4 | 5 | 6 | 7 | 8 | 9 | 10 | 11 | 12 |
| 0 | – | – | – | – | – | – | 445.67 [6] | – | – | – | – |
| 298[a] | 2.329 | – | 2.328 | 1.0153 | – | 358.30 | 442.46 | – | 98.74 | – | – |
| 1000[a] | – | – | 2.320 | – | – | – | 425.37 | – | – | – | – |
| 1300[a] | – | – | 2.305 | – | – | – | 417.22 | – | – | – | – |
| 1500[a] | – | – | 2.297 | – | – | – | 411.61 | – | – | – | – |
| 1690[a] | – | – | 2.285 | – | – | – | 405.25 | – | – | – | – |
| 1690 liq | 2.525 | – | – | 1.0185 | – | 355.90 | 356.00 | 30.4 | 28.2 | 25.3 | – |
| 1700 | 2.523 | 2.547 | – | 1.0211 | – | 355.71 | 355.65 | – | 37.4 | 24.2 | – |
| 1733 | 2.517 | | 2.515 | 1.0145 | 0.030 | 354.92 | 354.75 | 30.6 | – | 26.5 | – |
| 1750 | 2.516 | 2.534 | – | 1.0159 | – | 354.60 | 354.29 | – | 38.6 | – | – |
| 1800 | 2.508 | 2.520 | – | 1.0158 | – | 353.52 | 352.93 | 27.3 | 39.4 | 26.1 | 19–20 |
| 1900 | 2.491 | 2.494 | – | 1.0038 | – | 351.47 | 350.21 | | 39.8 | 26.6 | – |
| 2000 | 2.470 | 2.467 | – | 0.9999 | – | 349.34 | 347.49 | 27.6 | – | 32.3 | – |

[a] Crystal.

[b] Standard deviations grow from top to bottom from 0.073 to 0.079.

where η is the dynamic viscosity and $r_a$ is the atom radius. Choosing a value of 6.05 mP [4] for the viscosity at 1700 K and $r_a = 1.1 \times 10^{-8}$ cm (see above), we obtain $D = 1.9 \times 10^{-4}$ cm$^2$/s, which agrees with the actual value $(1.9 - 2.0) \times 10^{-4}$ (Table 3). The fulfillment of the Stokes-Einstein equation means that there is no association sign between the real liquid and, consequently, the computer model.

Thus, the simulation results show that the properties of liquid silicon are well described within the framework of the theory of simple liquids with a potential close to the hard-sphere potential, with a diameter of spheres being 2.20 Å. This diameter is smaller than the interatomic distance in the crystal (2.352 Å).

When simulating liquid silicon, we can use the pair contribution to the EAM potential given as a piecewise continuous polynomial [29, 36] rather than as a data table. We mark consecutive $k$ intervals on the abscissa axis $r$ by the division points $r_1 > 0$, $r_2$, $r_3$ ...$r_{k+1}$. The coordinate $r_1$ should be slightly smaller than the minimum interatomic distance $r_{min}$. The first interval is enclosed between the points $r_1$ and $r_2$. The coordinate $r_{k+1}$ must equal the cut-off radius of the potential $r_c$. The Schommers algorithm yields the values of the potential in the intervals from the first to the $k$th, i.e., for $r_1 \leqslant r \leqslant r_{k+1}$, and it does not work at distances $r < r_1$. At $r > r_1$, the potential is described by the expression

$$\varphi(r),\ \text{eV} = \sum_{i=1}^{k}\sum_{m=0}^{n} d_{im}\,(r - r_{i+1\blacklozenge})^m\, H\left(r_i, r_{i+1}\right), \quad (7)$$

where $i$ is the number of the interval on the distance axis, $dim$ are the coefficients of the series expansion, and the Heaviside function $H(r_i, r_{i+1})$ equals 1 in the interval $ri \leqslant r \leqslant r_{i+1}$ and zero in other intervals. For all $r = ri$, the potential itself and its first derivative are continuous. The distance $r$ is given in Å. The degree of the polynomials is $n$. In the case of silicon, $n = 7$, $k = 4$ is chosen. The coefficients $dim$ were obtained in the data approximation program (Table 1) and are given in Table 4. In this procedure, the potential values were reliably determined for distances $r \geqslant r_1 = 2.15$ Å, which actually occurred in the silicon model at 1733 K.

Since the minimum interatomic distances $r$min decrease at high temperatures and pressures, we need to

**Table 4.** Expansion coefficients of the pair contribution to the EAM potential of silicon

| $a_{im}$ | Interval number $i$ / Interval boundaries $r_i - r_{i+1}$, Å | | | |
|---|---|---|---|---|
| | 1 / 2.10 – 2.90 | 2 / 2.90 – 4.20 | 3 / 4.20 – 6.00 | 4 / 6.00 – 8.85 |
| $a_{i0}$ | –0.97113050520420D–01 | 0.31690669711679D–02 | –0.31873278785497D–02 | 0.00000000000000D+00 |
| $a_{i1}$ | 0.21899378299713D+00 | 0.12773799896240D+00 | 0.34430783707649D–02 | 0.00000000000000D+00 |
| $a_{i2}$ | –0.62291081298754D+01 | 0.27154179420195D–01 | 0.84230139063026D–01 | –0.35165857912545D–01 |
| $a_{i3}$ | –0.79015407873123D+02 | 0.43481827129286D+00 | 0.56141844748633D+00 | –0.13246413781381D+00 |
| $a_{i4}$ | –0.41364497186011D+03 | 0.13526037867501D+01 | 0.11214214299747D+01 | –0.16534787554672D+00 |
| $a_{i5}$ | –0.10115477873406D+04 | 0.14864527900288D+01 | 0.89595677539435D+00 | –0.93427224218695D–01 |
| $a_{i6}$ | –0.11462934613386D+04 | 0.74986992706763D+00 | 0.31125775931700D+00 | –0.24739723425154D–01 |
| $a_{i7}$ | –0.48846592560798D+03 | 0.15751335772576D+00 | 0.39450678719440D–01 | –0.24982008692301D–02 |

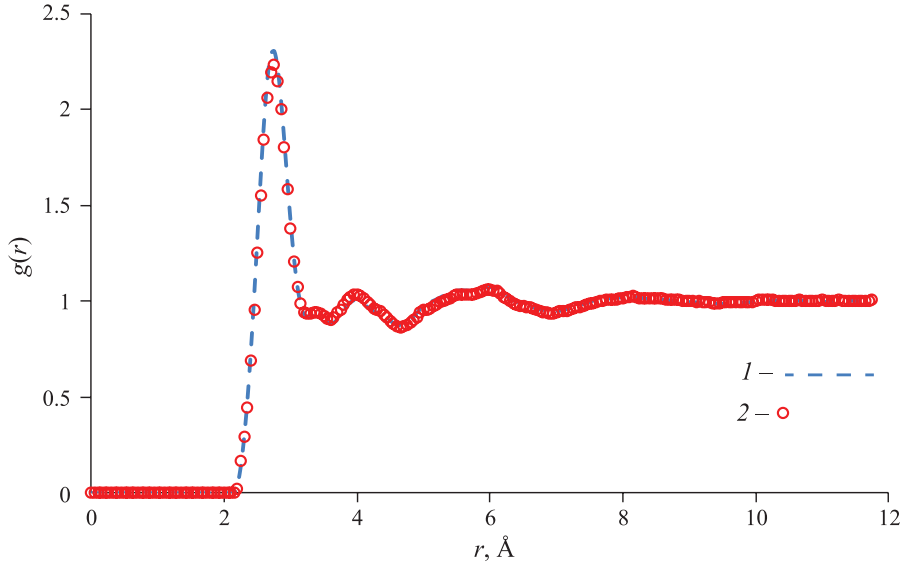


**Fig. 5.** PCF of liquid germanium — (1) diffraction data at 1253 K [1], and (2) model with the EAM potential. Residual $R_g = 0.020$.

extrapolate the potential to distances smaller than *r*min. For silicon, it is assumed that when $r < r_1$,

$$\varphi(r),\ \text{eV} = \varphi\left(2.15\ \text{Å}\right) + $$
$$+\left(-502.94 \cdot r^3 + 3292.6 \cdot r^2 - 7183.9 \cdot r + 5223.7\right),$$

where $r$ is expressed in Å and $\varphi(2.15\ \text{Å}) = -0.0787061$ eV. The transition to writing the potential in form (7) results in a small loss of accuracy, so that the residual $R_g$ of the function $g(r)$ of silicon at 1733 K increases from 0.023 to ~0.06.

**Simulating germanium**. Solid germanium is a semiconductor. The crystalline lattice is the same as that of silicon. Diffraction data on the structure of liquid germanium are given in [1, 33, 37], and at pressures up to 25 GPa they are given in [38]. The pair correlation function of germanium at 1253 K is shown in Fig. 5. The first peak at 2.75 Å is quite high and narrow, so that the first coordination sphere is well defined, with its radius being 3.60 Å. The average coordination number CN = 8.63 ± 1.41. There are data on the density of solid and liquid germanium up to 1900 K [4, 5, 9, 39], compressibility [40], energy of germanium up to 2000 K [6], viscosity [39, 41], self-diffusion coefficients [10, 33, 42], properties at high pressures [11, 43, 44], shock compression [12, 45], etc.

A considerable number of works are devoted to simulating liquid germanium with SW-type potentials [14, 15, 33, 46], Tersoff potentials [18], and strong bond

**Table 5.** Pair contribution to the potential of liquid germanium. Schommers algorithm at 1253 K. Pair correlation function [1] with correction [50], residual $R_g = 0.020$

| $r$, Å | φ($r$), eV | $r$, Å | φ($r$), eV | $r$, Å | φ($r$), eV | $r$, Å | φ($r$), eV |
|---|---|---|---|---|---|---|---|
| 1.5 | 122.300000 | 3.35 | –0.046844 | 5.2 | 0.002804 | 7.05 | 0.000684 |
| 1.55 | 101.303000 | 3.4 | –0.047240 | 5.25 | 0.001824 | 7.1 | 0.000647 |
| 1.6 | 82.303100 | 3.45 | –0.046399 | 5.3 | 0.000588 | 7.15 | 0.000611 |
| 1.65 | 65.292800 | 3.5 | –0.044678 | 5.35 | –0.001230 | 7.2 | 0.000504 |
| 1.7 | 50.263000 | 3.55 | –0.043242 | 5.4 | –0.003176 | 7.25 | 0.000431 |
| 1.75 | 37.220100 | 3.6 | –0.042177 | 5.45 | –0.005154 | 7.3 | 0.000489 |
| 1.8 | 26.207900 | 3.65 | –0.042683 | 5.5 | –0.006862 | 7.35 | 0.000379 |
| 1.85 | 17.311800 | 3.7 | –0.044350 | 5.55 | –0.008321 | 7.4 | 0.000296 |
| 1.9 | 10.611500 | 3.75 | –0.046536 | 5.6 | –0.009686 | 7.45 | 0.000160 |
| 1.95 | 6.066300 | 3.8 | –0.048615 | 5.65 | –0.010724 | 7.5 | 0.000095 |
| 2.00 | 3.391330 | 3.85 | –0.050613 | 5.7 | –0.011583 | 7.55 | –0.000021 |
| 2.05 | 2.031660 | 3.9 | –0.051642 | 5.75 | –0.012469 | 7.6 | 0.000084 |
| 2.1 | 1.338040 | 3.95 | –0.051700 | 5.8 | –0.013597 | 7.65 | 0.000363 |
| 2.15 | 0.847698 | 4.00 | –0.050500 | 5.85 | –0.014618 | 7.7 | 0.000651 |
| 2.2 | 0.407810 | 4.05 | –0.048100 | 5.9 | –0.015344 | 7.75 | 0.000941 |
| 2.25 | 0.242786 | 4.1 | –0.044900 | 5.95 | –0.015799 | 7.8 | 0.001186 |
| 2.3 | 0.163421 | 4.15 | –0.041400 | 6 | –0.015927 | 7.85 | 0.001263 |
| 2.35 | 0.098270 | 4.2 | –0.037700 | 6.05 | –0.015415 | 7.9 | 0.001323 |
| 2.4 | 0.045892 | 4.25 | –0.034200 | 6.1 | –0.014349 | 7.95 | 0.001494 |
| 2.45 | 0.002577 | 4.3 | –0.030800 | 6.15 | –0.013169 | 8 | 0.001467 |
| 2.5 | –0.033705 | 4.35 | –0.027300 | 6.2 | –0.011718 | 8.05 | 0.001491 |
| 2.55 | –0.063315 | 4.4 | –0.023400 | 6.25 | –0.009987 | 8.1 | 0.001490 |
| 2.6 | –0.086566 | 4.45 | –0.018900 | 6.3 | –0.008416 | 8.15 | 0.001489 |
| 2.65 | –0.103683 | 4.5 | –0.014400 | 6.35 | –0.007194 | 8.2 | 0.001543 |
| 2.7 | –0.114948 | 4.55 | –0.010100 | 6.4 | –0.006185 | 8.25 | 0.001735 |
| 2.75 | –0.120340 | 4.6 | –0.006120 | 6.45 | –0.005239 | 8.3 | 0.001765 |
| 2.8 | –0.120399 | 4.65 | –0.002540 | 6.5 | –0.004468 | 8.35 | 0.001859 |
| 2.85 | –0.115695 | 4.7 | –0.000011 | 6.55 | –0.003829 | 8.4 | 0.001948 |
| 2.9 | –0.107163 | 4.75 | 0.001530 | 6.6 | –0.003287 | 8.45 | 0.001727 |
| 2.95 | –0.095625 | 4.8 | 0.002330 | 6.65 | –0.002381 | 8.5 | 0.001419 |
| 3 | –0.082393 | 4.85 | 0.002780 | 6.7 | –0.001598 | 8.55 | 0.001148 |
| 3.05 | –0.069123 | 4.9 | 0.002900 | 6.75 | –0.000845 | 8.6 | 0.000767 |
| 3.1 | –0.057489 | 4.95 | 0.002840 | 6.8 | –0.000322 | 8.65 | 0.000519 |
| 3.15 | –0.049449 | 5 | 0.002930 | 6.85 | 0.000049 | 8.7 | 0.000388 |
| 3.2 | –0.045410 | 5.05 | 0.003130 | 6.9 | 0.000385 | 8.75 | 0.000199 |
| 3.25 | –0.044939 | 5.1 | 0.003420 | 6.95 | 0.000652 | 8.8 | 0.000043 |
| 3.3 | –0.045923 | 5.15 | 0.003320 | 7 | 0.000703 | 8.85 | 0.000000 |

**Table 6.** Liquid germanium. Parameters of the embedded potential

| | | | |
|---|---|---|---|
| $p_1$ | 0.57450 | $n$ | 2048 |
| $p_2$ | 0.80 | $dr$, Å | 0.05 |
| $\rho_1$ | 0.875 | $r_0$, Å | 9.86 |
| $\rho_2$ | 1.125 | $r_c$, Å | 8.96 |
| $a_1$ | –2.7455, eV | $c_1$, eV | 1.5559 |

**Table 7.** Decomposition coefficients of the pair contribution to the EAM potential of germanium

| $a_{im}$ | Interval number $i$ / Interval boundaries $r_i - r_{i+1}$, Å | | | |
|---|---|---|---|---|
| | 1/2.10–2.80 | 2/2.80–4.20 | 3/4.20–6.00 | 4/6.00–8.95 |
| $a_{i0}$ | –0.12914022803307D+00 | 0.31741657294333D–02 | –0.34244309645146D–02 | 0.00000000000000D+00 |
| $a_{i1}$ | 0.36918279528618D+00 | 0.12768036127090D+00 | 0.16339456196874D–02 | 0.00000000000000D+00 |
| $a_{i2}$ | –0.78049397398888D+01 | –0.12277981456606D+00 | 0.80042188493656D–01 | –0.29761810826526D–01 |
| $a_{i3}$ | –0.10718496961367D+03 | –0.65316546093368D+00 | 0.55860454460684D+00 | –0.12030635388921D+00 |
| $a_{i4}$ | –0.56677608973579D+03 | –0.15237788383222D+01 | 0.11235902756831D+01 | –0.15270893689047D+00 |
| $a_{i5}$ | –0.14389761345321D+04 | –0.20467986563964D+01 | 0.90001319360143D+00 | –0.86186740805348D–01 |
| $a_{i6}$ | –0.17372676812327D+04 | –0.12959413204484D+01 | 0.31329384464215D+00 | –0.22597590985478D–01 |
| $a_{i7}$ | –0.80443673950751D+03 | –0.29391029780645D+00 | 0.39797389267772D–01 | –0.22478041469157D–02 |

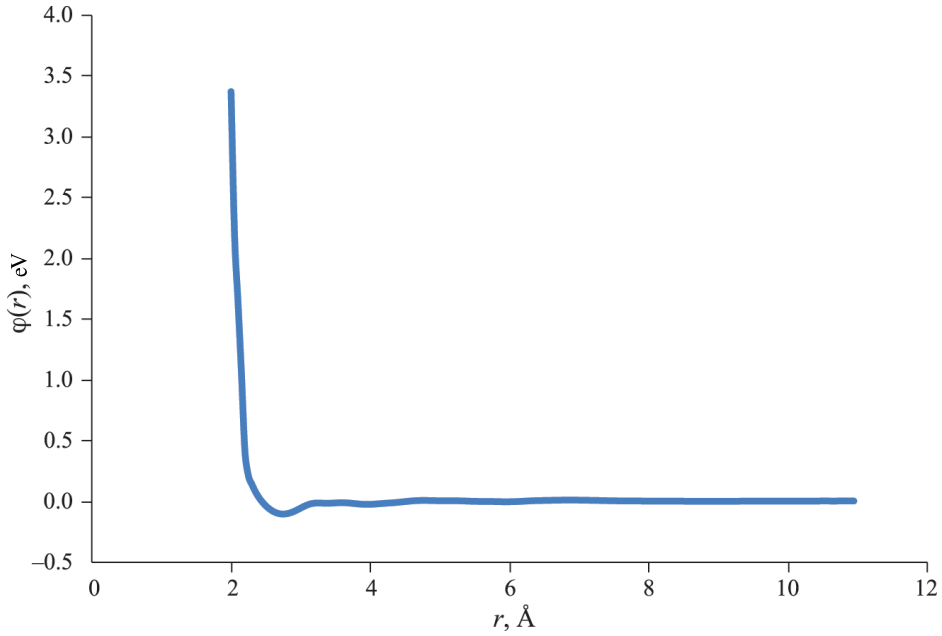


**Fig. 6.** Pair contribution to the EAM potential of germanium, 1253 K.

potentials [44]. A number of potentials are given in the NIST repository [22]. The MEAM potential was also applied in [18, 24, 47], the machine learning potential was applied in [48], and the ab initio method was applied in [44, 49]. The average CN of liquid germanium (8.63) is higher than that of silicon, so that the contribution of the covalent bond is smaller in germanium. Hence, the EAM potential for liquid germanium may be quite suitable.

We determined the pair contribution to the EAM potential for germanium using the Schommers algorithm, similar to the case of silicon. The PCF of liquid Ge at 1253 K was calculated using the structure factor [1] with the least squares method involved [50]. The liquid model of 2048 atoms was constructed in 154 iterations with the final residual $R_g = 0.020$. As we can see from Fig. 5, the real and model PCF are in good agreement. The pair contribution to the EAM potential of liquid Ge is shown in Fig. 6 and given in Table 5. It is also similar to the hard-sphere one with a step down. The parameters of the embedded potential are given in Table 6.

When modeling liquid germanium, one can also use the pair contribution to the EAM potential given as a piecewise continuous polynomial (7) rather than a data table. In the case of germanium, we chose $n = 7$, $k = 4$. The coefficients in formula (7) for germanium are given in Table 7.

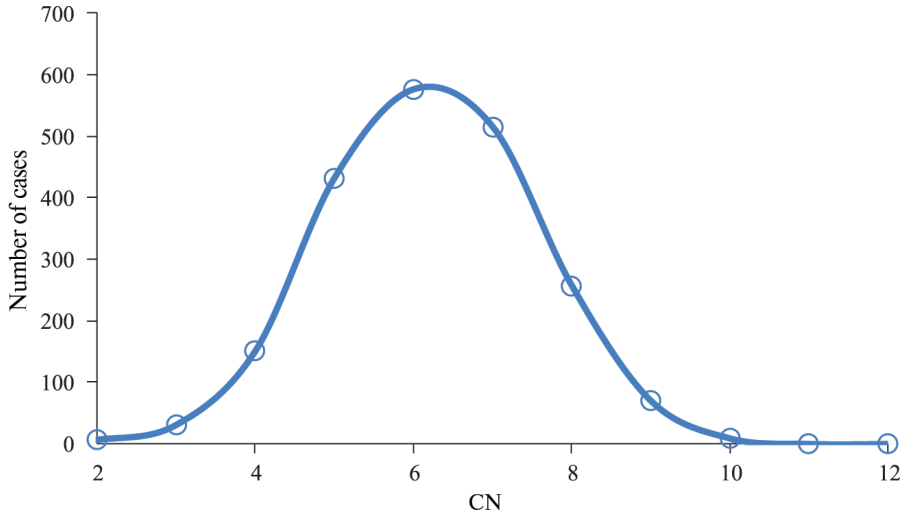


**Fig. 7.** Coordination numbers of the germanium model at 1253 K. Radius of the sphere of nearest neighbors is 3.6 Å.

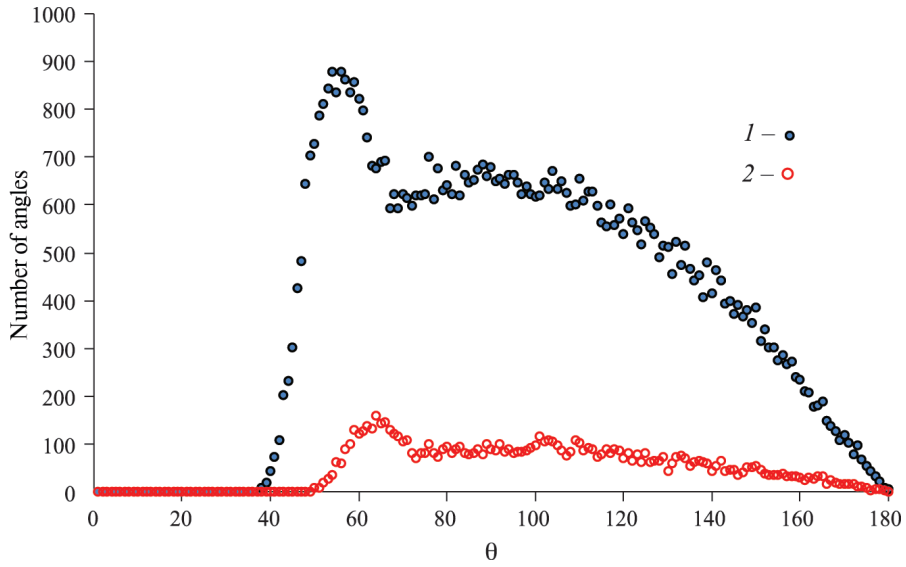


**Fig. 8.** Azimuth angles in the Ge model at 1253 K — (1) radius of the nearest neighbor sphere 3.6 Å, and (2) sphere radius 2.8 Å.

This potential works in the interval 2.20–8.95 Å. An upward branch should be smoothly added to it at $r < 2.20$ Å.

Using the EAM potential, we constructed a series of liquid germanium models consisting of 2048 atoms in a basic cube with periodic boundary conditions, at temperatures 1200–1800 K, in the *NVT* and *NpT* modes. The pair correlation function $g(r)$ at 1253 K is shown in Fig. 5 in excellent agreement with diffraction data [1].

Figure 7 shows the distribution of CN of liquid germanium atoms at 1253 K calculated with the radius of the nearest-neighbor sphere of 3.20 Å. It has a form characteristic of simple metals and passes through the maximum when $Z = 6$. The average value of $Z = 6.17 \pm 1.35$. Choosing the radius of the sphere of nearest neighbors to be 3.60 Å, we have $Z = 8.63 \pm 1.41$. As in the case of silicon, predominantly tetrahedral packing is not observed. The distribution of CN in germanium is very similar to the case of silicon.

The distribution of azimuth angles also looks similar to silicon (Fig. 8), but with the maximum shifted from the value 60° in silicon to the value 56°. For a smaller sphere radius of 2.8 Å, the first maximum is at the angle 65°. In the *ab initio* method [51], the angle distribution is similar, but at the radius 2.8 Å, the first maximum at 80° is much lower than the second maximum (at 100°). The tetrahedral angle at 109° is still quite far away.

**Table 8.** Properties of Ge models constructed by the MD method at $p$ ~0.001 GPa

| $T$, K | $d$, g/cm$^3$ | | | | <ρ>[b] | $R_g$ | $-E$, kJ/mol | | $K_T$, GPa | | $D \times 10^5$, cm$^2$/s | |
|---|---|---|---|---|---|---|---|---|---|---|---|---|
| | MD | Exp [52] | Exp [5] | Exp [39] | | | $-E_{MD}$ | $-E_{exp}$ [6] | MD | Exp [31] | MD | Exp [10] |
| 1 | 2 | 3 | 4 | 5 | 6 | 7 | 8 | 9 | 10 | 11 | 12 | 13 |
| 0 | – | – | – | – | – | – | – | 369.04 | – | – | – | – |
| 298[a] | – | – | 5.372 | – | – | – | 236.01 | 364.40 | – | – | – | – |
| 673 | – | – | 5.333 | – | – | – | – | – | – | – | – | – |
| 1153 | – | – | 5.284 | – | – | – | – | – | – | – | – | – |
| 1200 | 5.542 | – | – | 5.58 | – | – | 277.44 | 341.05 | – | – | 10.1 | 13.0 |
| $1210.4_{sol}$ | – | – | – | – | – | – | | 340.76 | – | – | – | – |
| $1210.4_{liq}$ | 5.526 | – | – | – | 1.00741 | – | 303.67 | 303.73 | – | – | – | – |
| 1253 | 5.510 | 5.47 | 5.49 | 5.556 | 1.00467 | 0.019 | 302.75 | 302.72 | 30.8 | 31.5 | 11.9 | 13.9 |
| 1300 | 5.485 | 5.45 | 5.46 | 5.535 | 1.00070 | 0.021 | 301.54 | 301.26 | – | 31.3 | 12.5 | 14.6 |
| 1400 | 5.436 | 5.41 | 5.43 | 5.487 | 0.99540 | – | 299.08 | 298.50 | – | 30.4 | 14.0 | 16.2 |
| 1500 | 5.387 | 5.35 | – | 5.445 | 0.98453 | – | 296.82 | 295.74 | 28.2 | 29.7 | 15.8 | 17.6 |
| 1600 | 5.342 | 5.30 | – | 5.400 | 0.97576 | – | 294.46 | 292.98 | – | – | 17.3 | 19.0 |
| 1700 | 5.295 | 5.26 | – | 5.352 | 0.96786 | – | 292.17 | 290.02 | – | – | 18.6 | 22 [51] |
| 1800 | 5.236 | 5.22 | – | 5.32 | 0.95652 | – | 289.72 | 287.49 | – | – | 19.5 | – |
| 1900 | 5.178 | 5.16 | – | – | 0.94962 | – | 287.37 | 284.70 | – | – | – | – |
| 2000 | 5.135 | – | – | – | 0.94245 | – | 285.18 | 281.94 | 18.7 | – | – | 23 [51] |

The behavior of the structure of liquid Si and Ge as compared to what we see for the SW and Ter potentials indicates the weakening of the covalent bond when the elements are shifted from top to bottom in the Periodic System, from silicon to germanium.

The results of calculations of liquid germanium properties in the *NpT* mode at temperatures up to 2000 K are given in Table 8. Published data on the density show a significant scatter. The best agreement is obtained with the data of [5, 52]. There is also good agreement with the experiment on the PCF form at 1253 K (the small residual $R_g = 0.020$), as well as with *ab initio* PCF at 2000 K [51]. The discrepancy with the experiment in terms of model energies is only 3 kJ/mol at 2000 K (electron energies not taken into account). The heat capacity of liquid germanium is close to 23 J/(mol K), i.e., to the classical value $3R$. The real heat capacity of liquid germanium is slightly higher, 27.6 J/mol/K.

The speed of sound in liquid germanium was measured in [31] at temperatures 1215–1443 K. At 1253 K, the adiabatic compressibility is $\beta s = 2.52 \times 10^{-11}$ m$^2$/N, so the adiabatic compressive modulus $K_s = 1/\beta s = 39.7$ GPa. According to MD data, the heat capacity ratio $C_p/C_v = 1.26$. Accordingly, the isothermal modulus is $K_T = K_s C_v/C_p = 31.5$ GPa. For $c_1 = 1.5559$, the value of the model modulus found from the pressure-volume relationship is $K_T = 30.8$ GPa. When heated from 1690 to 2000 K, the modulus of the model $K_T$ decreases to 18.7 GPa.

The closeness of the liquid germanium potential to the hard-sphere potential (see Fig. 6) allows us to verify formula (5) for the self-diffusion coefficient. Taking the diameter of the hard sphere $\sigma = 2.45$ Å, we find for the model at 1253 K $N/V = 0.045719$ at/Å3, $n = 0.6723$, $D_0 = (3/8) \times 2.45 \times 10^{-8} \times (8.31 \times 10^7 \times 1253/\pi/72.59)^{1/2} = 1.9632 \times 10^{-4}$ cm$^2$/s, and finally $D_{HS} = 1.13 \times 10^{-4}$ cm$^2$/s. This value agrees well with $1.19 \times 10^{-4}$ obtained by the MD method. Calculations by the *ab initio* method yield at 1250 K a close value $D = 0.95 \times 10^{-4}$ cm$^2$/s [49]. The pseudopotential calculation yields $1.27 \times 10^{-4}$ [53]. The results of direct measurements of self-diffusion in liquid germanium are close to those given above (see Table 8).

As a result, we have that the properties of liquid germanium are well described by the EAM potential, which is close to the hard-sphere potential with a step down.

## DISCUSSION OF RESULTS

Previously, it was shown by the *ab initio* method that at high pressures a chemical bond between two atoms in liquid silicon arises spontaneously due to a random approach of these atoms to a distance less than 2.5 Å [21]. In this work, we showed that the behavior of liquid silicon and germanium models is well described by EAM potentials with almost complete disappearance of directionality of the bond. For the coordination numbers 6 and higher, the locally isotropic short-range order turns out to be more favorable. As a result, hybridization of electronic states of the $sp^3$ type in liquid silicon and germanium is not realized. Many properties of liquid silicon and germanium are consistent with the concept of isotropic interaction. Hence, potentials generating directionality of the bond in crystals (SW, Ter, etc.) should be of little use for simulating liquid silicon and germanium at densities close to ordinary ones. This explains the relatively low accuracy of the potentials proposed to describe simultaneously the solid and liquid phases of silicon and germanium.

We apply this reasoning, for instance, for carbon located above silicon in the Periodic System. When moving up the 4th group of elements, the ionization potentials of atoms grow (from 7.90 in germanium to 8.15 eV in silicon and 11.3 in carbon) and, accordingly, the limits of temperatures and pressures increase, at which gradual transitions from the directional bond in carbon (of the $sp$, $sp^2$ or $sp^3$ type) to the isotropic structure of liquid carbon should occur as the density grows. Such a transition is observed when simulating carbon by the *ab initio* method at 9000 K and densities above 5.8 g/cm$^3$ [54]. Staying within the framework of classical molecular dynamics, one should expect a smooth change of the interparticle potential at compression from the oprion of directional bond (SW type) to the isotropic potential. In the transition region, it can be realized, for instance, as a sum of these two potentials with weights depending on the liquid density.

Roughly, when the density decreases by a factor of 2–3 (due to heating), the mentioned transition can occur in silicon and germanium in the opposite direction, viz. from an isotropic liquid near the melting point to a liquid with the directional bond. This prediction can be easily verified by the *ab initio* method.

## REFERENCES


1. *Waseda Y.* The Structure of Non-Crystalline Materials. Liquids and Amorphous Solids. N.Y.: McGraw-Hill, 1980.
2. *Funamori N., Tsuji K.* // Phys. Rev. Lett. 2002. Vol. 88. P. 255508.
3. *Demchuk T., Bryk T., Seitsonen A.P. et al.* // DOI.org/10.48550/arXiv.2009.00834.
4. *Assael M.J., Armyra I.J., Brillo J. et al.* // J. Phys. Chem. Ref. Data. 2012. Vol. 41. No. 3. DOI.org/10.1063/1.4729873.
5. *Glazov V.M., Chizhevskaya S.N., Glagoleva N.N.* Liquid semiconductors. Moscow: Nauka, 1967.
6. *Gurvich L.A., Veyts I.V., Medvedev V.A. et al.* Thermodynamic properties of individual substances. Vol. 2. Book 2. Moscow: Nauka, 1979.
7. *Desai P.D.* // J. Phys. Chem. Ref. Data. 1986. Vol. 15. No. 3. P. 967.
8. *Tekuchev V.V.* Acoustic and physicochemical properties of electron melts. Volgograd. 2016.
9. *Regel A.R., Glazov V.M.* Physical properties of electron melts. Moscow: Nauka, 1980.
10. *Weis H., Kargl F., Kolbe M. et al.* // J. Phys.: Condens. Matter. 2019. Vol. 31. P. 455101.
11. *Luo Sheng-Nian, Ahrens T.J., Asimow P.D.* // J. Geophys. Res. 2003. Vol. 108. No. B9. P. 2421. DOI:10.1029/2002JB002317.
12. *Oleynik I.I., Zybin S.V., Elert M.L., White C.T.* // CP845 "Shock Compression in Condensed Matter". Ed. M.D. Furnish et al. 2005. P. 413.
13. *Stillinger F.H., Weber T.A.* // Phys. Rev. B. 1985. Vol. 31. P. 5262.
14. *Dziedzic J., Principi E., Rybicki J.* // J. Non-Cryst. Solids. 2006. Vol. 352. P. 4232.
15. *Jadhav P.P., Dongale T.D., Vhatkar R.S.* // AIP Conference Proceedings 2162, 020038 (2019); DOI.org/10.1063/1.5130248
16. *Tersoff J.* // Phys. Rev. B. 1988. V. 38. P. 9902; 1989. Vol. 39. P. 5566.
17. *Ishimaru M., Yoshida K., Motooka T.* // Phys. Rev. B. 1996. Vol. 53. No. 11. P. 7176.
18. *Cook S.J., Clancy P.* // Phys. Rev. B. 1993. Vol. 47. P. 7686.
19. *Bazant M.Z., Kaxiras E.* // Phys. Rev. Lett. 1996. Vol. 77. P. 4370.
20. *Luo J., Zhou Ch., Cheng Y., Liu L.* // J. Crystal Growth. 2020. P. 1. DOI: 10.1016/j.jcrysgro.2020.125785
21. *Štich I., Car R., Parrinello M.* // Phys. Rev. B. 1991. Vol. 44. P. 4262.
22. NIST. IPS Interatomic Potentials Repository: www.ctcms.nist.gov/potentials/refs.html
23. *Baskes M.I.* // Phys. Rev. B. 1992. Vol. 46. P. 2727. DOI.org/10.1103/PhysRevB.46.2727.
24. Baskes *M.I., Nelson J.S., Wright A.F.* // Phys. Rev. B. Condens. Matter. 1989. Vol. 40. No. 9. P. 6085. DOI: 10.1103/physrevb.40.6085.
25. *Starikov S.V., Lopanitsyna N.Yu., Smirnova D.E., Makarov S.V.* // Computational Materials Science. 2018. Vol. 142. P. 303.

26. *Starikov S., Gordeev I., Lysogorskiy Yu. et al.* // Computational Materials Science. 2020. Vol. 184. P. 109891.
DOI: 10.1016/j.commatsci.2020.109891.
27. *Daw M.S., Baskes M.I.* // Phys. Rev. B. 1984. Vol. 29. No. 12. P. 6443.
28. *Schommers W.* // Phys. Rev. A. 1983. Vol. 28. P. 3599.
29. *Belashchenko David K.* Liquid Metals. From Atomistic Potentials to Properties, Shock Compression, Earth's Core and Nanoclusters. NOVA Science Publushers. NY.
30. *Zhu Z.G., Liu C.S.* // Phys. Rev. B. 2000. Vol. 61. No. 14. P. 9322.
31. *Hayashi M., Yamada H., Nabeshima N., Nagata K.* // Int. J. Thermophysics. 2007. Vol. 28. No. 1. P. 83. DOI: 10.1007/s10765-007-0151-9.
32. *Chelikowsky J.R., Troullier N., Binggeli N.* // Phys. Rev. B. 1994. Vol. 49. P**.** 114.
33. *Yu W., Wang Z.Q., Stroud D.* // Phys. Rev. B. 1996. Vol. 54. No. 19. P. 13946.
34. *Belashchenko D.K.* // Russ. J. Phys. Chem. 2019. Vol. 93. No. 6. Pp. 1093–1105.
35. *Speedy R.J.* // Mol. Physics. 1987. Vol. 62. No. 2. P. 509.
36. *Belashchenko D.K.* // Phys. Usp. 2013. Vol. 183. No. 12. P. 1176.
37. *Alteholz Th., Hoyer W.*// J. Non-Cryst. Solids. 1999. Vol. 250–252. P. 48.
38. *Petkov V., Takeda S., Waseda Y., Sugiyama K.* // J. Non-Cryst. Solids. 1994. Vol. 168. P. 97.
39. *Sato Y., Nishizuka T., Tachikawa T. et al.* // High Temperatures - High Pressures. 2000. Vol. 32. P. 253.
40. *Tsuchiya Y.* // J. Phys. Soc. Japan. 1991. Vol. 60. No. 1. P. 227.
41. *Masaki T., Itami T.* // "Modeling and Precise Experiments of Diffusion Phenomena in Melts under Microgravity" Annual Reports. 2002, NASDA-TMR-030005E.
42. *Kato M., Minowa S.* // Trans. Iron Steel Institute of Japan. 1969. Vol. 9. P. 39.
43. *Tsuji K., Mori T., Hattori T. et al.* // 2000B0087-CD-np BL04B1.
44. *Kōga J., Okumura H., Nishio K. et al.* // Phys. Rev. B. 2002. Vol. 66. P. 064211.
45. *Kishimura H., Matsumoto H., Thadhani N.N.* // J. Physics: Conference Series. 2010. Vol. 215. P. 012145;
DOI:10.1088/1742-6596/215/1/012145
46. *Ding K., Andersen H.C.* // Phys. Rev. B. 1986. Vol. 34. No. 10. P. 6987.
47. *Kim Eun Ha, Shin Young-Han, Lee Byeong-Joo* // Computer Coupling of Phase Diagrams and Thermochemistry. 2008. Vol. 32. P. 34.
48. *Zuo Y., Chen C., Li X. et al.* // J. Phys. Chem. A. 2019. Vol. 124. No. 4. P. 731.
DOI: 10.1021/acs.jpca.9b08723.
49. *Kresse G., Hafner J.* // Phys. Rev. B. 1994. Vol. 49. No. 20. P. 14251.
50. *Belashchenko D.K.* // Kristallographiya (Crystallography). 1998. Vol. 43. No. 3. P. 400.
51. *Kulkarni R.V., Aulbur W.G., Stroud D.* // Phys. Rev. B. 1997. Vol. 55. P**.** 6896.
52. *Lucas L.D., Urbain G.* // C. r. Acad. Sci. 1962. Vol. 255. No. 19. P. 2414.
53. *Munejiri S., Shimojo F., Hoshino K., Itami T.* // NASDA, Tsukuba 305-8505, Japan
54. *Hoshino K. // J. Phys.: Condens. Matter.* 2009. Vol. 21. No. 47. P. 474212.
DOI 10.1088/0953-8984/21/47/474212.